

REPORT 1273

A STUDY OF THE ZERO-LIFT DRAG-RISE CHARACTERISTICS OF WING-BODY COMBINATIONS NEAR THE SPEED OF SOUND¹

By RICHARD T. WHITCOMB

SUMMARY

Comparisons have been made of the shock phenomena and drag-rise increments for representative wing and central-body combinations with those for bodies of revolution having the same axial developments of cross-sectional areas normal to the airstream. On the basis of these comparisons, it is concluded that near the speed of sound the zero-lift drag rise of a low-aspect-ratio thin-wing and body combination is primarily dependent on the axial development of the cross-sectional areas normal to the airstream. It follows that the drag rise for any such configuration is approximately the same as that for any other with the same development of cross-sectional areas.

Investigations have also been made of representative wing-body combinations with the body so indented that the axial developments of cross-sectional areas for the combinations were the same as that for the original body alone. Such indentations greatly reduced or eliminated the zero-lift drag-rise increments associated with the wings near the speed of sound.

INTRODUCTION

In the interpretation of the zero-lift drag-rise characteristics of configurations near the speed of sound, the transonic similarity rules and linear theory have been applied in limited analyses. However, no general means is available for directly explaining quantitatively the variations of the transonic drag rise associated with the numerous changes in wing plan form and section considered by airplane designers even for the simplified case of a wing alone. More important, even a qualitative understanding of the large and highly variable zero-lift drag interferences near the speed of sound associated with practical combinations of wings and bodies has been lacking. A logical means for interpreting the drag-rise values for bodies with thin low-aspect-ratio wings is discussed herein.

The results presented in reference 1 indicate that, for a representative swept-wing and central-body combination, the zero-lift drag rise is due primarily to shock losses. A study of these results also indicates that the shock formations about this relatively complex configuration at zero lift near the speed of sound are similar to those that would be

expected for a body of revolution with the same axial development of cross-sectional areas normal to the airstream. Further, the drag-rise characteristics for this wing-body combination at zero lift are about the same as those for a body of revolution (ref. 2) with approximately the same axial development of cross-sectional areas. On the basis of these facts and a preliminary consideration of the general physical nature of the flow about configurations, it has been reasoned that near the speed of sound the zero-lift drag rise of a wing-body configuration generally should be primarily dependent on the axial development of the cross-sectional areas normal to the airstream.

In order to ascertain the soundness of this concept, measurements have been made of the flow fields and drag-rise characteristics for four representative wing—central-body combinations and for bodies of revolution with the same axial developments of cross-sectional areas normal to the airstream. The results, obtained at Mach numbers from 0.85 to 1.10 in the Langley 8-foot transonic tunnel, are compared and analyzed herein. In order to illustrate possibilities for improving airplane performance at transonic speeds, zero-lift drag coefficients for three special wing-body combinations are also presented.

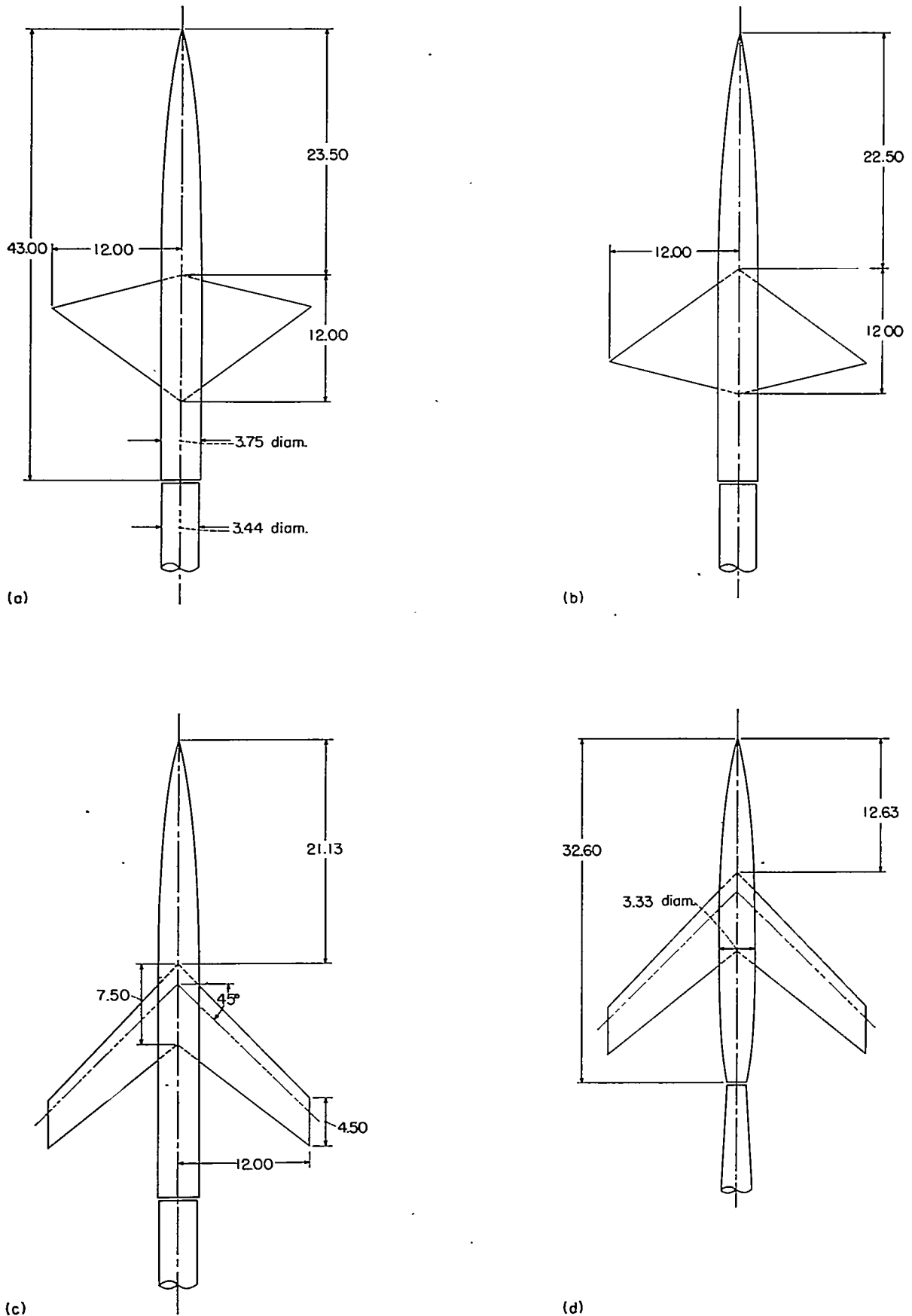
EXPERIMENTS AND PROCEDURE

CONFIGURATIONS

Basic bodies.—The major part of the results discussed herein were obtained for three wings in conjunction with the body of revolution shown in figures 1 (a), 1 (b), and 1 (c). The body is normally cylindrical in the region of the wing and has a forebody of the same shape as that of the body described in reference 1. The radii of the cylindrical body are given in table I. The swept wing was also investigated in conjunction with the body having a curved afterbody as shown in figure 1 (d). This combination is the same model used in studies in reference 1. Radii of the curved body are also given in table I. The maximum diameter of this curved body is somewhat less than that of the cylindrical body.

Wings.—The wing for which the most extensive results were obtained has 0° sweep of the quarter-chord line, an

¹ Supersedes recently declassified NACA Research Memorandum L62H08 by Richard T. Whitcomb, 1952



(a) Unswept wing, cylindrical body.
 (c) Swept wing, cylindrical body.

(b) Delta wing, cylindrical body.
 (d) Swept wing, curved body.

FIGURE 1.—Wing-body combinations used in investigation. (All dimensions are in inches.)

aspect ratio of 4.0, and a taper ratio of 0. The streamwise sections of the wing are symmetrical, are 4 percent thick, and consist of circular arcs with the maximum thickness at the 40-percent-chord stations. This configuration (fig. 1 (a)) is referred to as the "unswept" wing. Results were also obtained with this wing reversed so that the 75-percent-chord line is unswept, as shown in figure 1 (b). The leading-edge sweep of this wing is 37°. This configuration has almost a delta plan form and, therefore, is referred to as the "delta" wing. Finally, investigations were made with a wing which has 45° sweep of the quarter-chord line, an aspect ratio of 4.0, a taper ratio of 0.6, and an NACA 65A006 airfoil section parallel to the airstream. This configuration (figs. 1 (c) and 1 (d)) is referred to as the "swept" wing.

Special bodies.—Bodies of revolution with the same axial developments of cross-sectional areas as the wing-body combinations were obtained by altering the original bodies. The radii of these revised bodies of revolution are given in table II. Special indented bodies of revolution were investigated in conjunction with the three wings and these bodies were also obtained by altering the original cylindrical body. The radii of these bodies in the region of the wing are presented in table III.

MEASUREMENTS

Schlieren surveys were obtained with a temporary schlieren system. In order to obtain side-view schlieren surveys of the fields at distances from the model center lines with the horizontal symmetrically oriented schlieren system, the various models were displaced downward from the center line of the tunnel, as shown in figure 2 (a). In every case the displacements for the comparable bodies of revolution were the same as for the wing-body combination. Plan-view schlieren surveys for the unswept-wing—body configuration were obtained by rotating the model 90° and displacing it farther from the center line of the tunnel. Wall Mach number distributions were obtained from pressures measured at the rows of orifices placed along the center lines of panels of the test section adjacent to the top and bottom panels as shown in figure 2 (a). The relative radial locations of the wall Mach number measurement stations with respect to

TABLE II.—ORDINATES OF COMPARABLE BODIES OF REVOLUTION

[All dimensions are in inches]

Comparable to unswept wing on cylindrical body		Comparable to delta wing on cylindrical body	
Station	Radius	Station	Radius
22.500	1.875	22.500	1.875
23.500	1.875	24.000	1.875
24.500	1.893	24.500	1.882
25.000	1.939	25.000	1.894
25.500	2.012	25.500	1.911
26.000	2.087	26.000	1.934
26.500	2.165	26.500	1.968
27.000	2.182	27.000	1.992
27.500	2.185	27.500	2.019
28.000	2.174	28.000	2.054
28.500	2.145	28.500	2.086
29.000	2.113	29.000	2.113
29.500	2.088	29.500	2.145
30.000	2.054	30.000	2.174
30.500	2.019	30.500	2.185
31.000	1.992	31.000	2.182
31.500	1.968	31.500	2.155
32.000	1.934	32.000	2.087
32.500	1.911	32.500	2.012
33.000	1.894	33.000	1.939
33.500	1.882	33.500	1.892
34.000	1.875	34.500	1.875
43.000	1.875	43.000	1.875

Comparable to swept wing on cylindrical body		Comparable to swept wing on curved body	
Station	Radius	Station	Radius
22.500	1.875	14.000	1.573
23.125	1.875	14.300	1.580
24.125	1.907	14.625	1.595
25.125	1.957	15.625	1.670
26.125	2.024	16.625	1.747
27.125	2.080	17.625	1.830
28.125	2.117	18.625	1.903
29.125	2.143	19.625	1.943
30.125	2.135	20.625	1.966
31.125	2.107	21.625	1.949
32.125	2.083	22.625	1.901
33.125	2.071	23.625	1.857
34.125	2.045	24.625	1.822
35.125	2.001	25.625	1.766
36.125	1.946	26.625	1.684
37.125	1.899	27.625	1.545
38.125	1.876	28.625	1.413
38.375	1.875	29.625	1.292
43.000	1.875	29.875	1.260
		30.000	1.251
		32.000	1.010
		32.605	0.940

TABLE I.—ORDINATES OF BASIC BODY

[All dimensions are in inches]

Cylindrical body		Curved body	
Station	Radius	Station	Radius
0	0	0	0
.225	.04	.200	.092
.338	.134	.300	.119
.563	.193	.500	.171
1.125	.325	1.000	.289
2.250	.542	2.000	.482
3.375	.726	3.000	.645
4.500	.887	4.000	.788
6.750	1.167	6.000	1.037
9.000	1.391	8.000	1.236
11.250	1.559	10.000	1.386
13.500	1.683	12.000	1.496
15.750	1.770	14.000	1.573
18.000	1.828	16.000	1.625
20.250	1.864	18.000	1.657
22.500	1.875	20.000	1.667
43.000	1.875	22.000	1.663
		24.000	1.610
		26.000	1.537
		28.000	1.425
		30.000	1.261
		32.000	1.010
		32.605	0.940

TABLE III.—ORDINATES OF INDENTED BODIES

[All dimensions are in inches]

With unswept wing		With delta wing		With swept wing	
Station	Radius	Station	Radius	Station	Radius
22.500	1.875	22.500	1.875	22.500	1.875
24.000	1.875	24.000	1.875	23.125	1.875
24.500	1.857	24.500	1.888	24.125	1.842
25.000	1.807	25.000	1.856	25.125	1.787
25.500	1.720	25.500	1.837	26.125	1.710
26.000	1.622	26.000	1.812	27.125	1.641
26.500	1.531	26.500	1.773	28.125	1.592
27.000	1.476	27.000	1.743	29.125	1.560
27.500	1.470	27.500	1.710	30.125	1.572
28.000	1.487	28.000	1.664	31.125	1.611
28.500	1.633	28.500	1.642	32.125	1.640
29.000	1.680	29.000	1.580	33.125	1.656
29.500	1.642	29.500	1.533	34.125	1.638
30.000	1.664	30.000	1.487	35.125	1.740
30.500	1.710	30.500	1.470	36.125	1.802
31.000	1.743	31.000	1.476	37.125	1.850
31.500	1.773	31.500	1.521	38.125	1.874
32.000	1.812	32.000	1.623	38.375	1.875
32.500	1.837	32.500	1.720	43.000	1.875
33.000	1.856	33.000	1.807		
33.500	1.868	33.500	1.857		
34.000	1.875	34.000	1.875		
43.000	1.875	43.000	1.875		

the model are also indicated in this figure. For the side-view schlieren surveys, the distances from the model center lines to these stations were 35.5 and 52.8 inches; for the plan-view surveys, they were 31.2 and 58.0 inches. Drag measurements were obtained by internal strain-gage balances. Base pressures were also measured.

PRESENTATION OF RESULTS

Detailed flow surveys.—Composites of the schlieren photographs and the distributions of wall Mach number M_w for the unswept-wing and cylindrical-body combination, the comparable body of revolution, and the cylindrical body alone are presented in figure 2 for several stream Mach numbers M_∞ . The schlieren photographs presented above the diagrams of the three configurations show the side views; those below the wing-body configuration show the plan views. The plan-view schlieren surveys for the wing-body configurations were not duplicated for the bodies of revolution. The relative orientations and sizes of the photographs with respect to the configuration outlines are the same as those of the schlieren fields with respect to the test model. (See sketches in fig. 2 (a).)

The wall Mach number distributions shown above the composites for the three configurations were obtained during side-view schlieren surveys; those below the composites for the wing-body combination are from plan-view surveys. (See sketches in fig. 2 (a).) These two Mach number distributions presented on a given set of ordinates (fig. 2) are for the two measurement stations that are shown by the circle and square symbols labeled in the top sketch of figure 2 (a). The Mach number distributions are placed on the composites so that the distances from the center line of the model to the M_w points on the Mach number scales are equal relatively to the distances from the model to the lower-wall Mach number measurement stations, as indicated by the circle symbol in the sketch in figure 2 (a). The horizontal scale of the wall Mach number distributions is the same as that for the model outline.

The stream Mach numbers M_∞ at which the various schlieren photographs and wall Mach number distributions were obtained varied by as much as ± 0.005 from the mean values for each of the composites. However, the maximum difference between the stream Mach number for the directly comparable side-view photographs for the wing-body combination and for the comparable body of revolution was approximately 0.003.

Drag coefficients.—The zero-lift drag coefficients C_{D_0} for the wing-body combinations, the comparable bodies of revolution, and the basic bodies alone, as presented in the various figures such as figure 3, are all based on wing areas of 1 square foot. These coefficients have been corrected to a condition at which the base pressure is equal to the stream static pressure. The drag-coefficient increments ΔC_{D_0} , as presented in figure 3, have been obtained by subtracting the drag-coefficient values measured at a Mach number of approximately 0.85 from those measured at the higher Mach numbers. This subtraction nearly eliminated the effects of differences in the skin friction of the comparable configura-

tions on the comparisons of the drag characteristics for these configurations.

The maximum error of the absolute drag coefficients presented is approximately ± 0.0005 . The effects of wall-reflected disturbances on the drag results have been essentially eliminated at all Mach numbers except those near a value of about 1.05. This elimination has been accomplished by displacing the model from the tunnel center line, by using a cylindrical afterbody on the larger body, and by correcting for the base-pressure variations. No results were obtained for Mach numbers near 1.05.

Schlieren photographs.—The schlieren fields for the delta- and swept-wing configurations (fig. 4, for example) were oriented with respect to the configurations as indicated by the lowest schlieren photographs and configuration outlines.

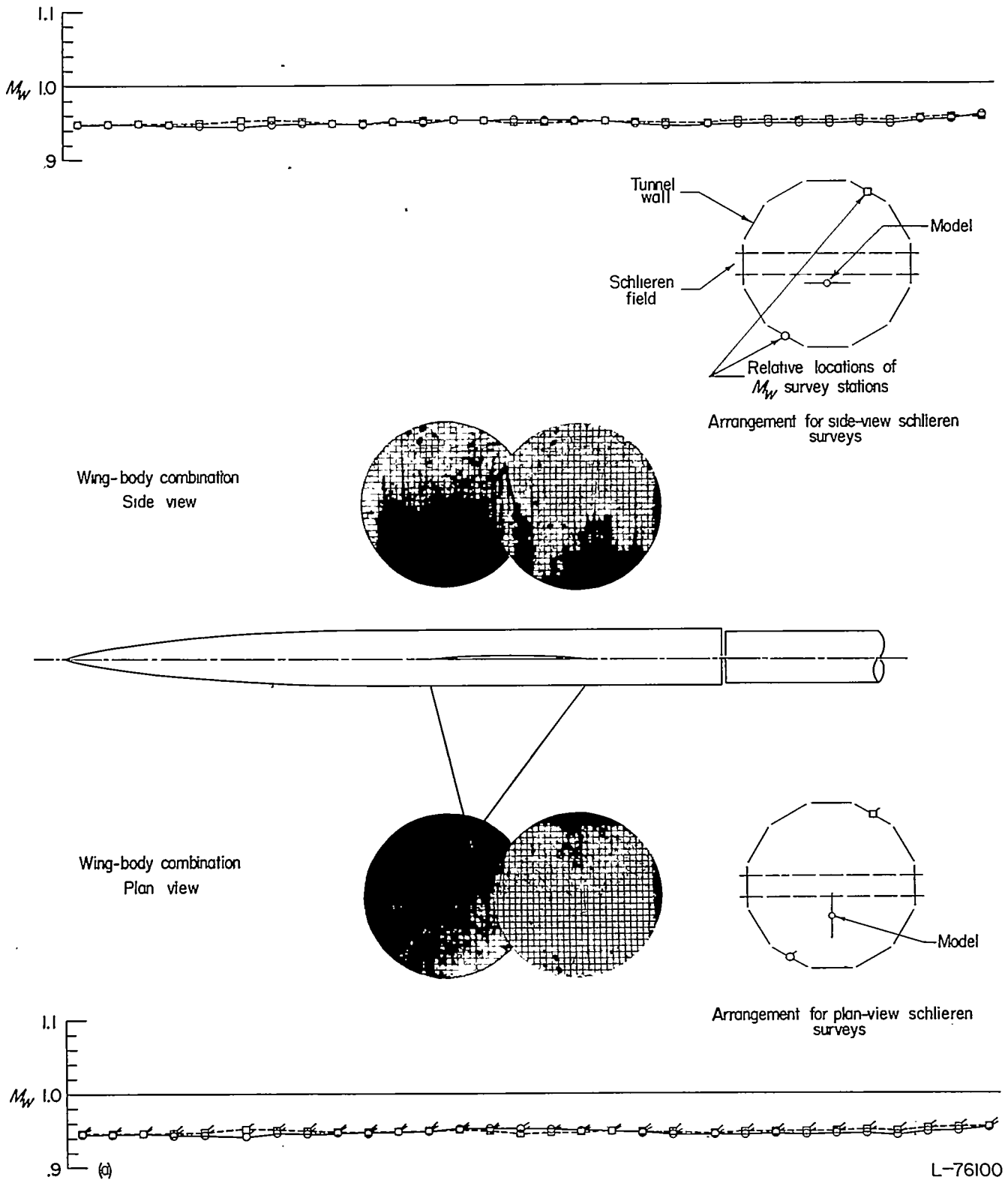
RESULTS AND DISCUSSION

In the discussion that follows, the basic comparisons and analyses are made for the unswept-wing—cylindrical-body combination. The results for the other combinations indicate the effects of several variations of the wing and body configurations on the phenomena.

UNSWEPT WING AND CYLINDRICAL BODY

Shock phenomena.—The wall Mach number distributions and schlieren photographs presented in figures 2 (a) to 2 (d) indicate that the extensive shock formations produced by the unswept-wing—cylindrical-body combination at the test Mach numbers near the speed of sound are almost exactly the same as those caused by the body of revolution with the same axial development of cross-sectional areas, except in the local region directly downstream of the wing. In this locality, the shock formations, while not as closely similar as at greater distances from the configurations, are at least approximately comparable. (The incompatible shock crossing the downstream, plan-view schlieren photograph (fig. 2 (d)), at a Mach number of 1.03 is a weak reflection of a disturbance of the configuration from the tunnel wall.) At a Mach number of 1.10 (fig. 2 (e)), the similarities of the schlieren photographs for the comparable configurations are less close than at Mach numbers near 1.0.

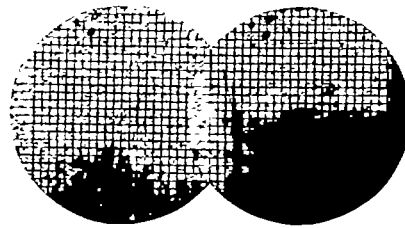
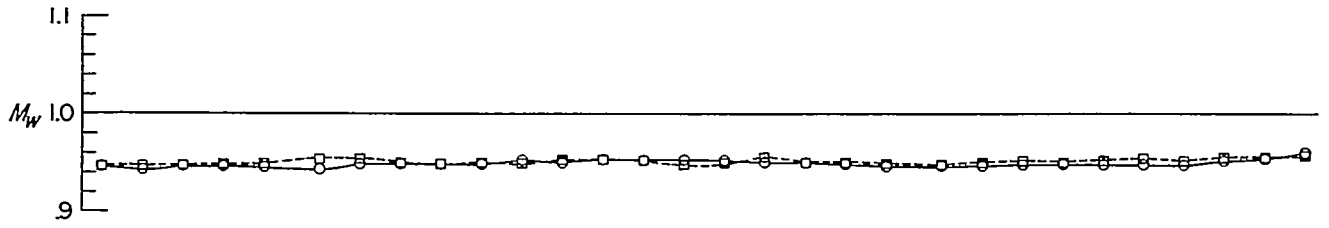
A study of the physical nature of the flow indicates that the similarities of the extensive shock formations produced by the wing-body combination and a body of revolution with the same axial development of cross-sectional areas near the speed of sound can logically be attributed primarily to two basic factors: the negligible variations of stream-tube areas with changes in velocity (ref. 3) and the concentration of the effects of a disturbance in a plane nearly normal to the airstream. (These two factors are basically related.) It is apparent that, because of the second factor, the streamwise locations of the effects of the disturbances of the wing should be essentially the same as those for the corresponding effects produced by the body of revolution with the same axial distribution of disturbances. Also, because of the second factor, the analysis of the lateral similarities of the fields of the comparable configurations may be greatly simplified by considering the flow changes in each normal plane independently.



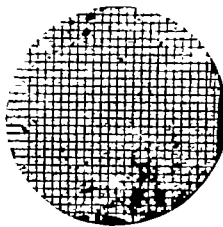
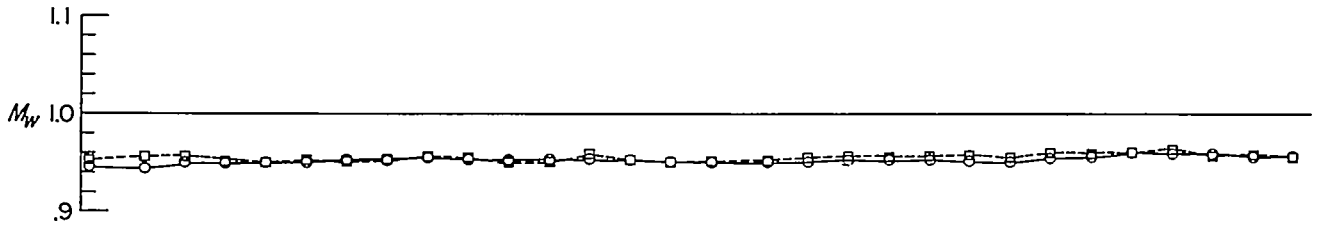
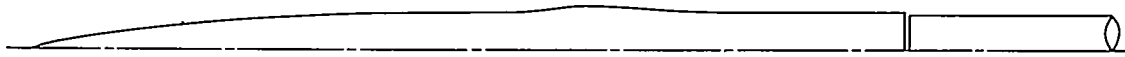
(a) $M_\infty = 0.95$.

L-76100

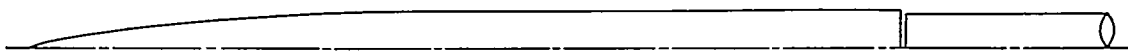
FIGURE 2.—Comparisons of the shock phenomena for the unswept-wing and cylindrical-body combination with those for the comparable body of revolution and the cylindrical body alone.



Comparable body of revolution
Side view



Cylindrical body
Side view

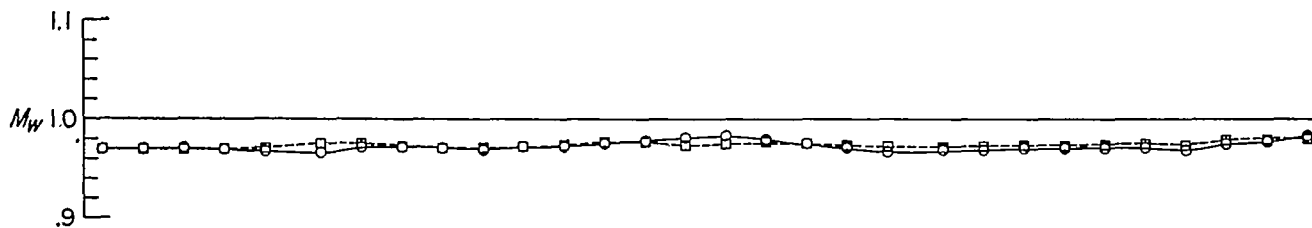


(a)

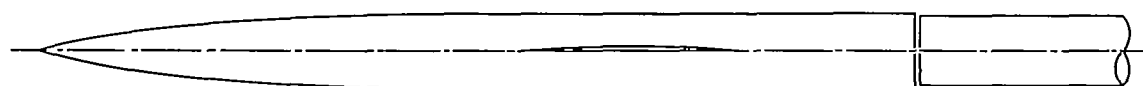
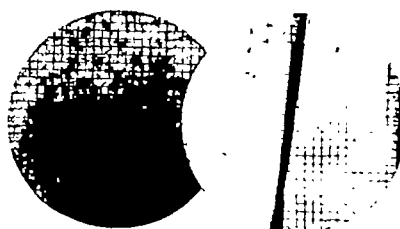
L-76101.1

(a) $M_\infty = 0.95$. Concluded.

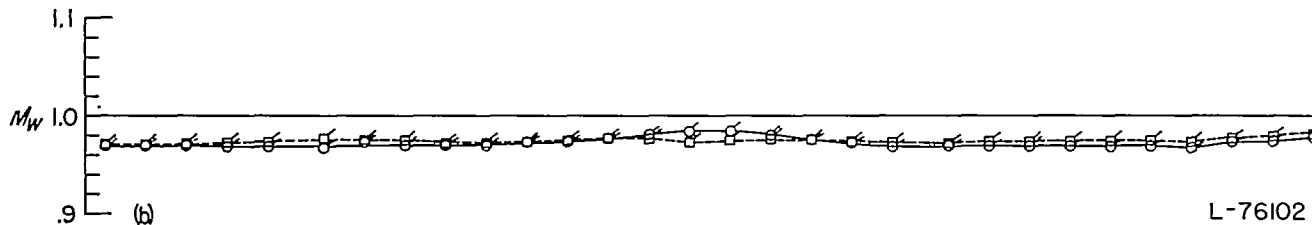
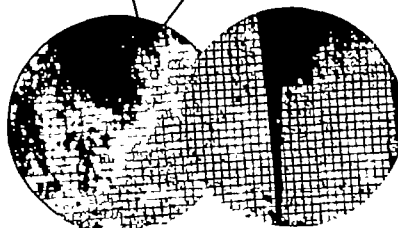
FIGURE 2.—Continued.



Wing-body combination
Side view



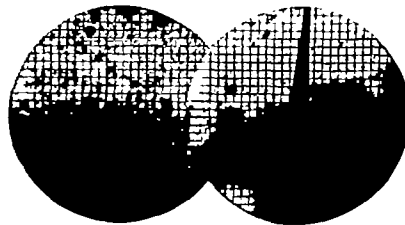
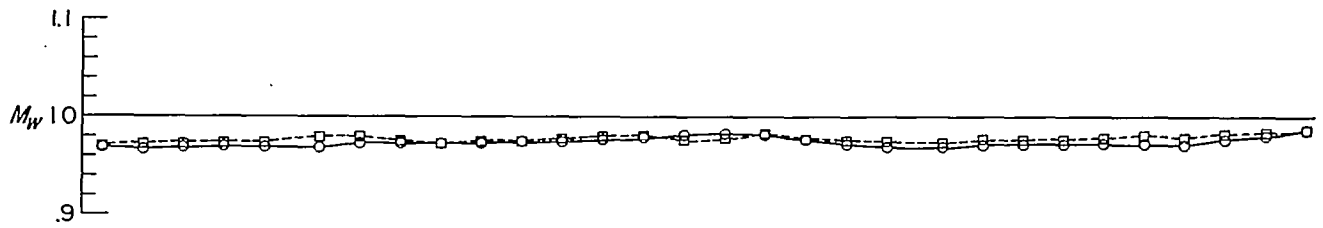
Wing-body combination
Plan view



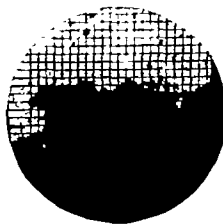
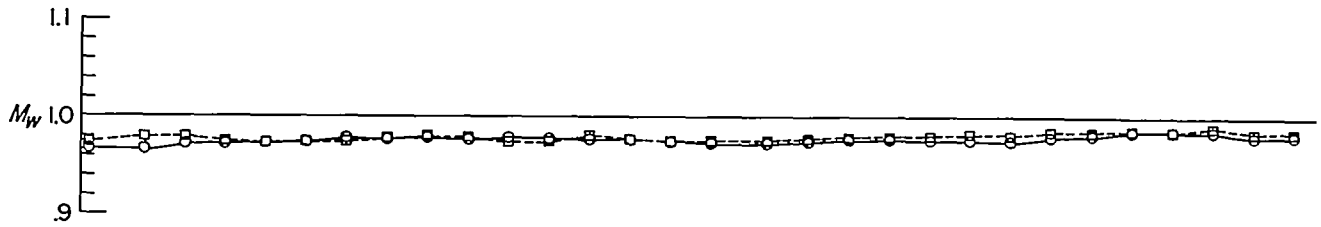
(b) $M_\infty = 0.98$. See figure 2 (a) for test-point arrangement.

L-76102

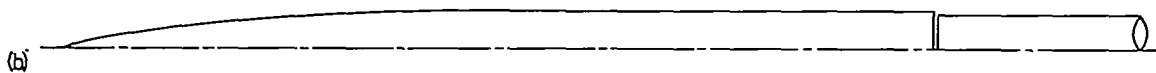
FIGURE 2.—Continued.



Comparable body of revolution
Side view



Cylindrical body
Side view

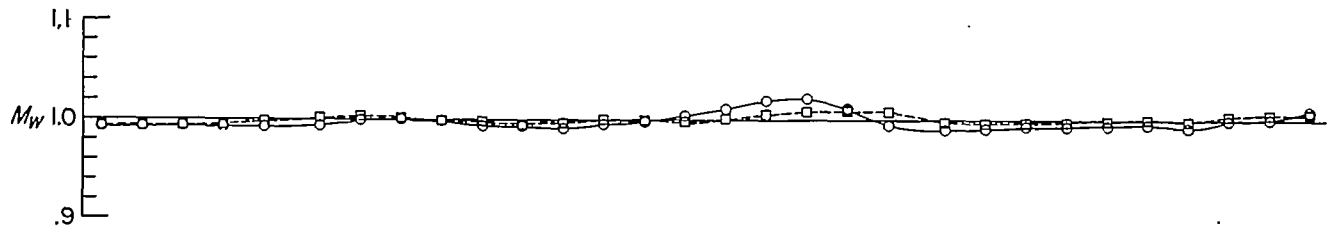


(b)

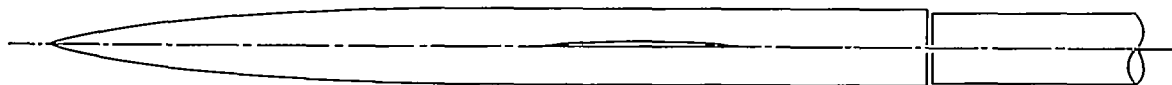
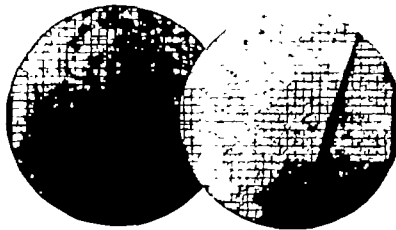
L-76103

(b) $M_\infty = 0.98$. Concluded.

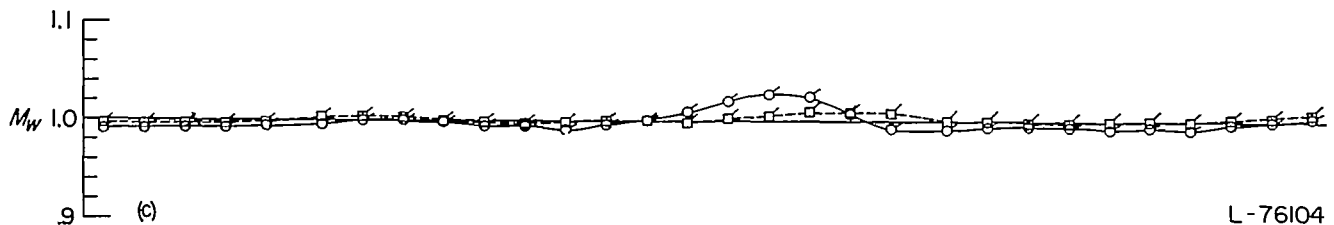
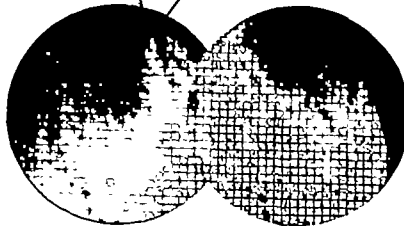
FIGURE 2.—Continued.



Wing-body combination
Side view



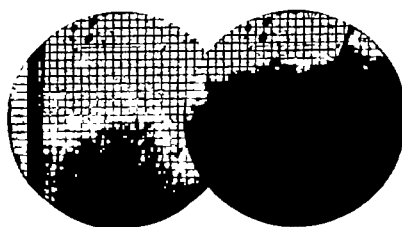
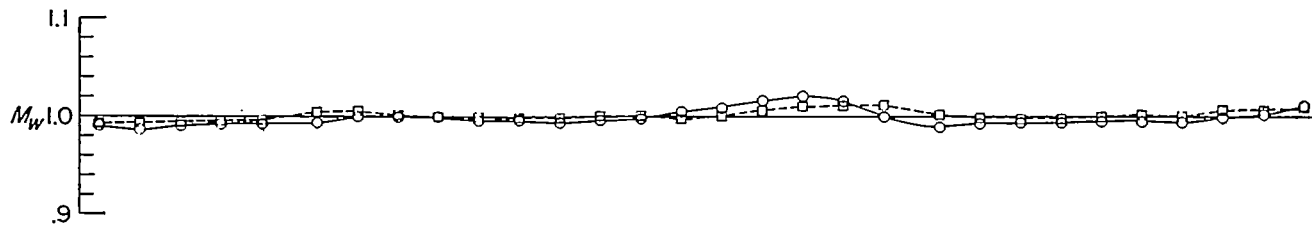
Wing-body combination
Plan view



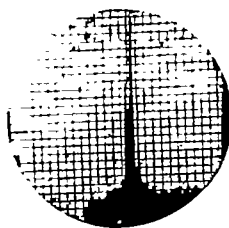
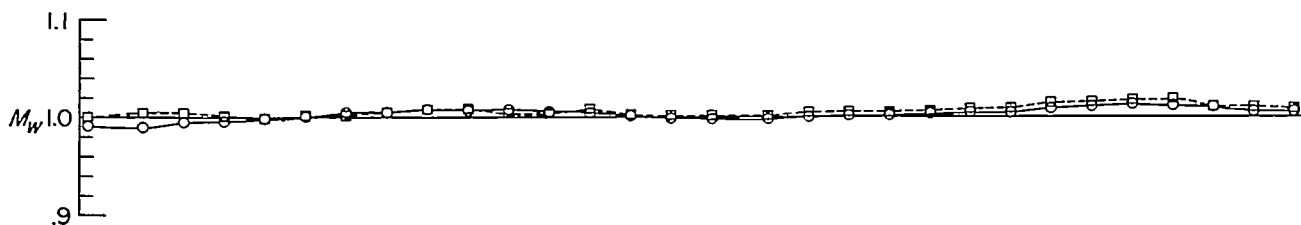
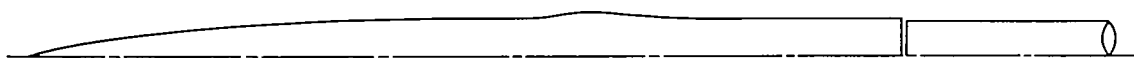
(c) $M_\infty = 1.00$. See figure 2 (a) for test-point arrangement.

L-76104

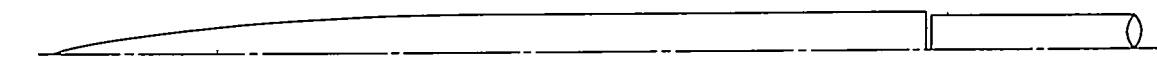
FIGURE 2.—Continued.



Comparable body of revolution
Side view



Cylindrical body
Side view

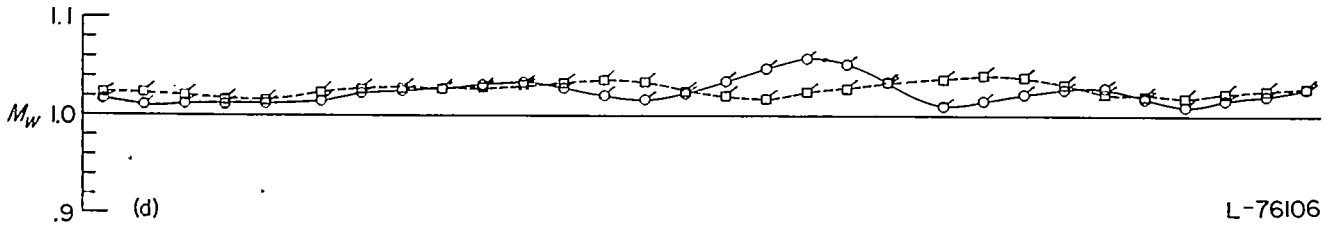
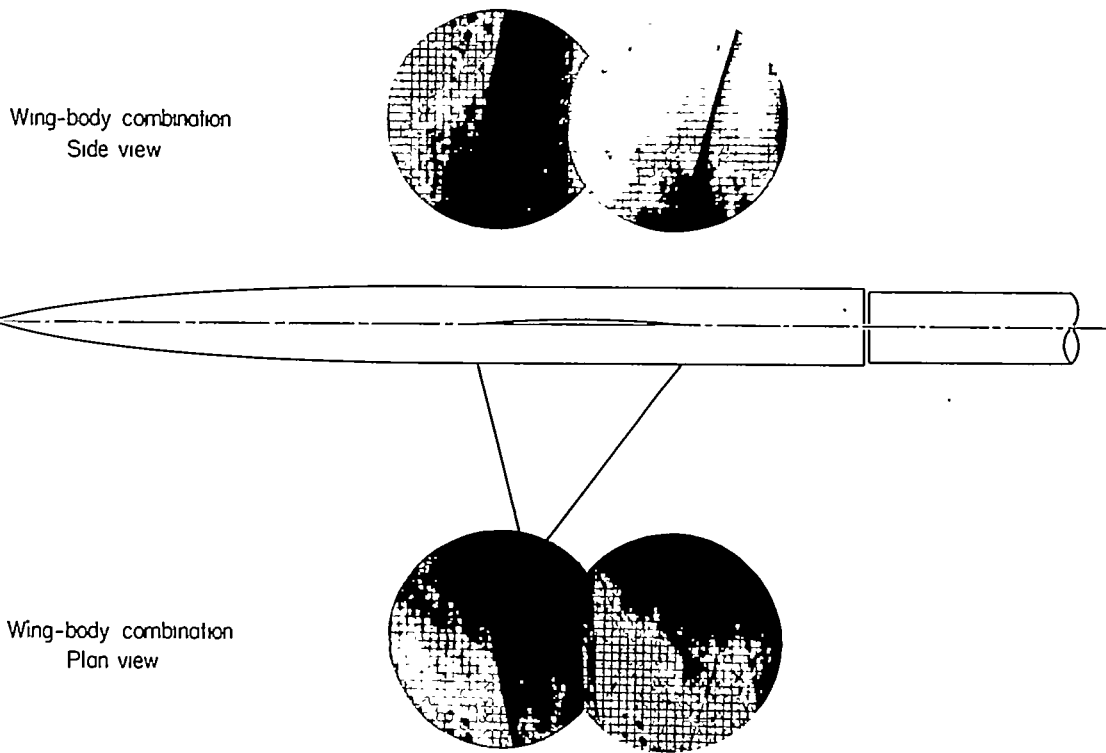
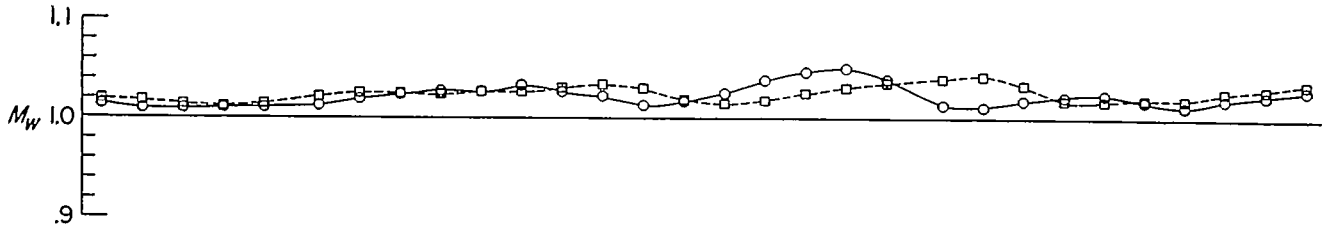


(c)

L-76105

(c) $M_\infty = 1.00$. Concluded.

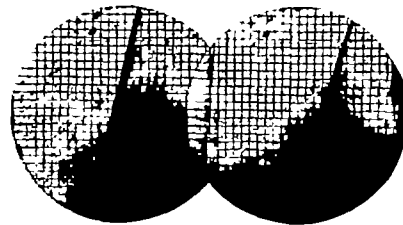
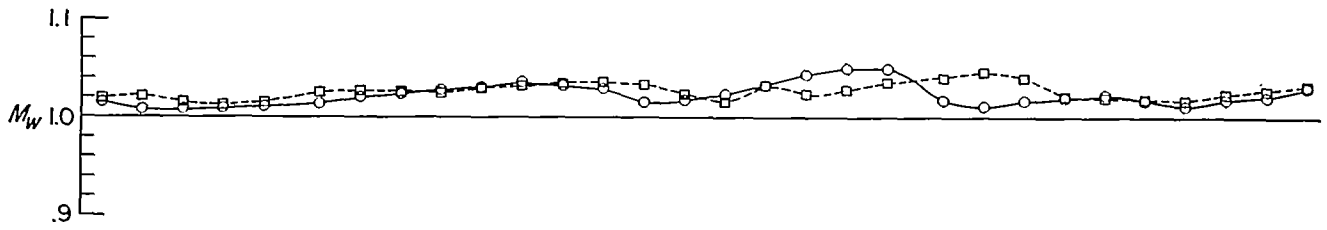
FIGURE 2.—Continued.



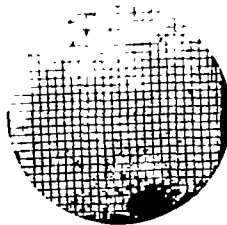
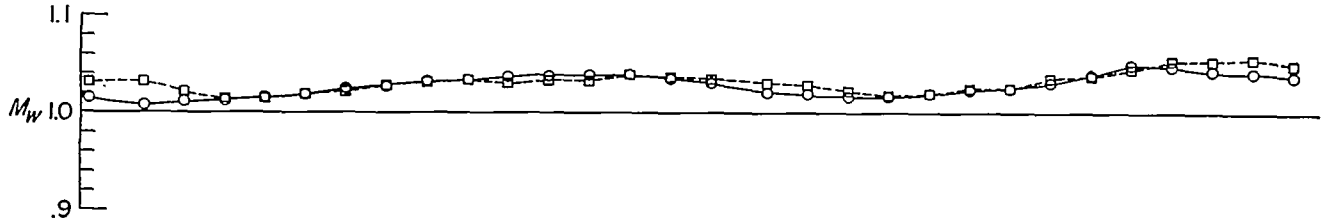
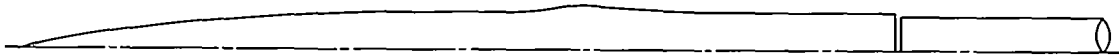
(d) $M_\infty=1.03$. See figure 2 (a) for test-point arrangement.

FIGURE 2.—Continued.

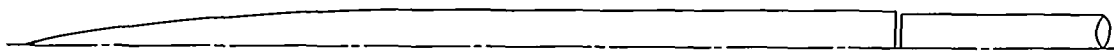
L-76106



Comparable body of revolution
Side view



Cylindrical body
Side view

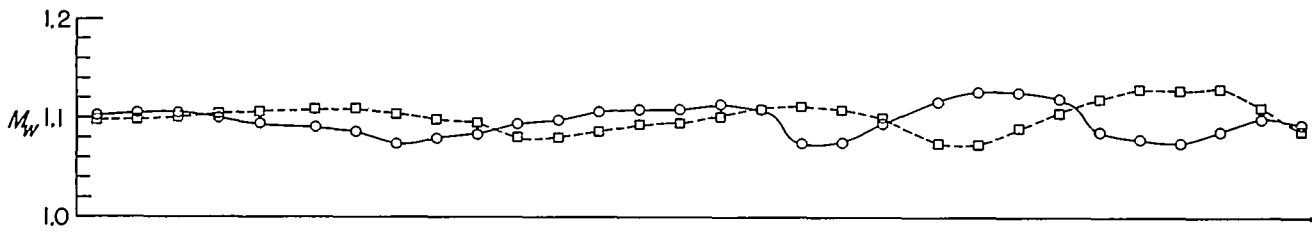


L-76107

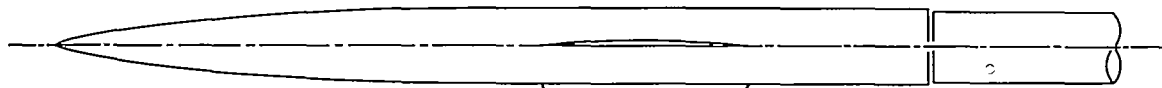
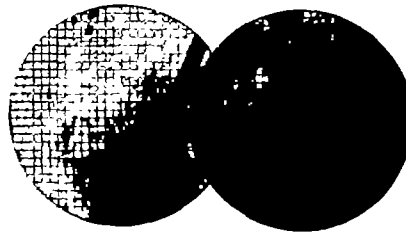
(d)

(d) $M_\infty = 1.03$. Concluded.

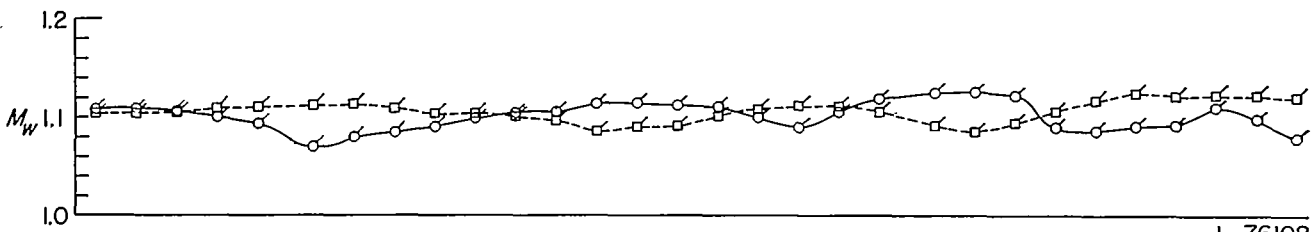
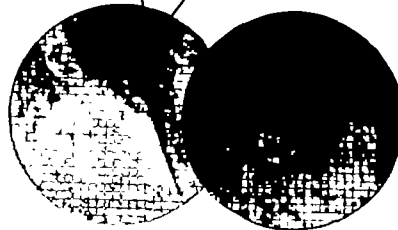
FIGURE 2.—Continued.



Wing-body combination
Side view



Wing-body combination
Plan view

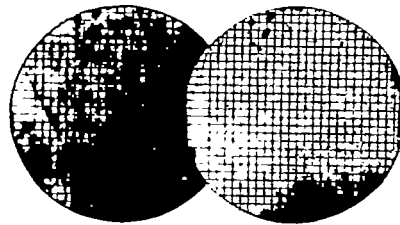
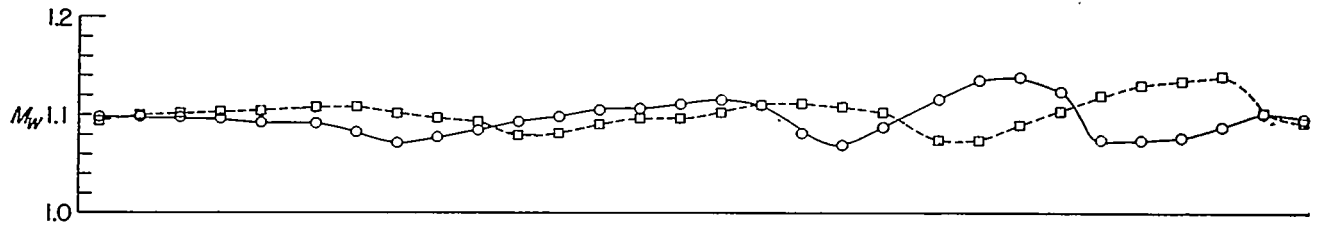


(e)

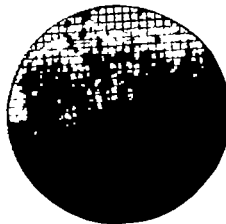
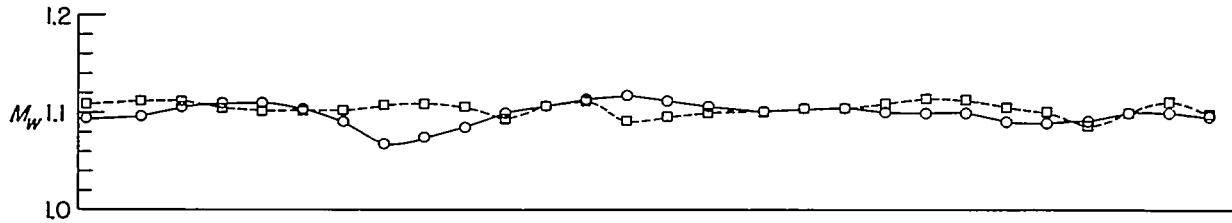
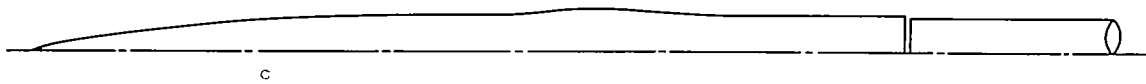
(e) $M_\infty = 1.10$. See figure 2 (a) for test-point arrangement.

L-76108

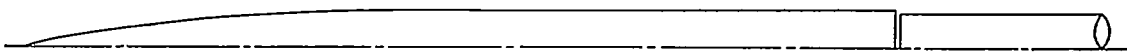
FIGURE 2.—Continued.



Comparable body of revolution
Side view



Cylindrical body
Side view



L-76109

(e)

(e) $M_w = 1.10$. Concluded.

FIGURE 2.—Concluded.

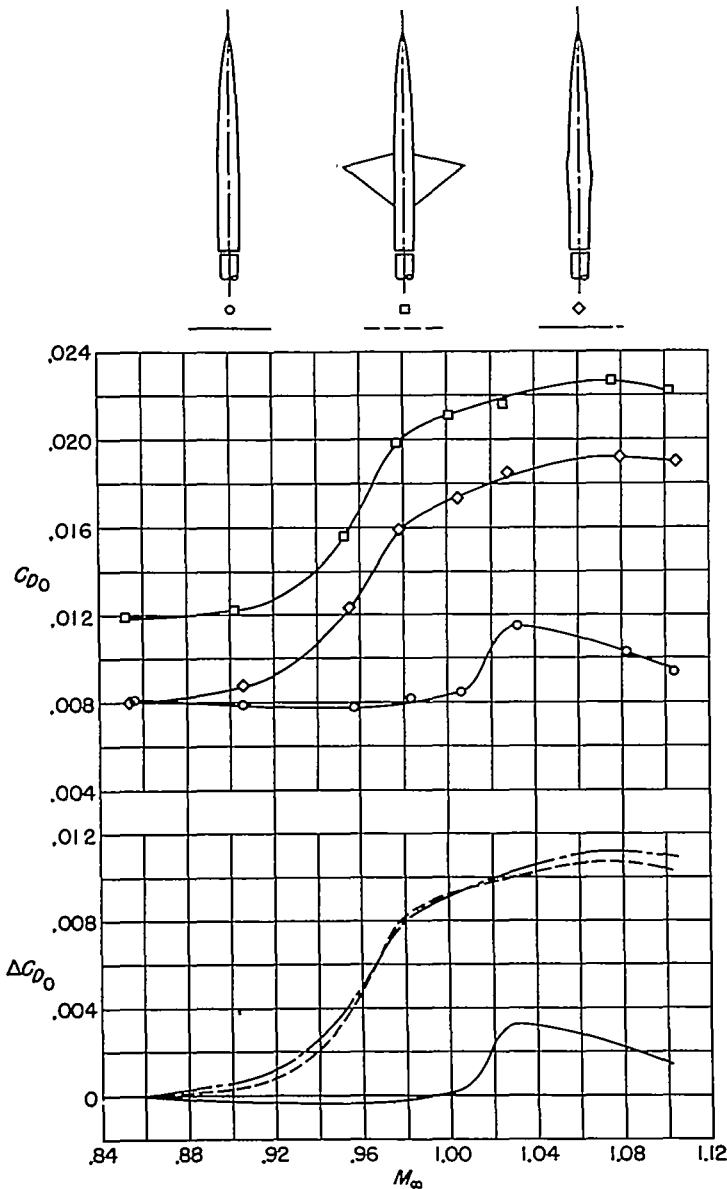


FIGURE 3.—Comparisons of the drag rise for the unswept-wing and cylindrical-body combination with that for the comparable body of revolution and the cylindrical body alone.

As a starting point for the analysis of the lateral similarities, consider the flow about the comparable configurations in a given normal plane at a circle, concentric to the axis of symmetry, outside the tip of the wing. As a result of the essential invariance of the stream tubes, the total radial deviations of the fields at this circle are essentially the same as the displacements of the surfaces of the configurations in the same plane. Since the total surface displacements for the two configurations are the same, the total flow deviations at the circle must be essentially equal. However, circumferential variations of these deviations may exist for the wing-body configuration. The essential irrotationality of the flow leads to reductions of these circumferential variations with increase in distance from the configuration. Because of the invariance of the stream-tube areas, these reductions are relatively rapid. This invariance causes the outer field to be relatively inflexible, and as a result, it reacts strongly to the circumferential variations of the radial deviations; this reaction produces pronounced circumferential pressure gradients. These gradients cause deviations in the

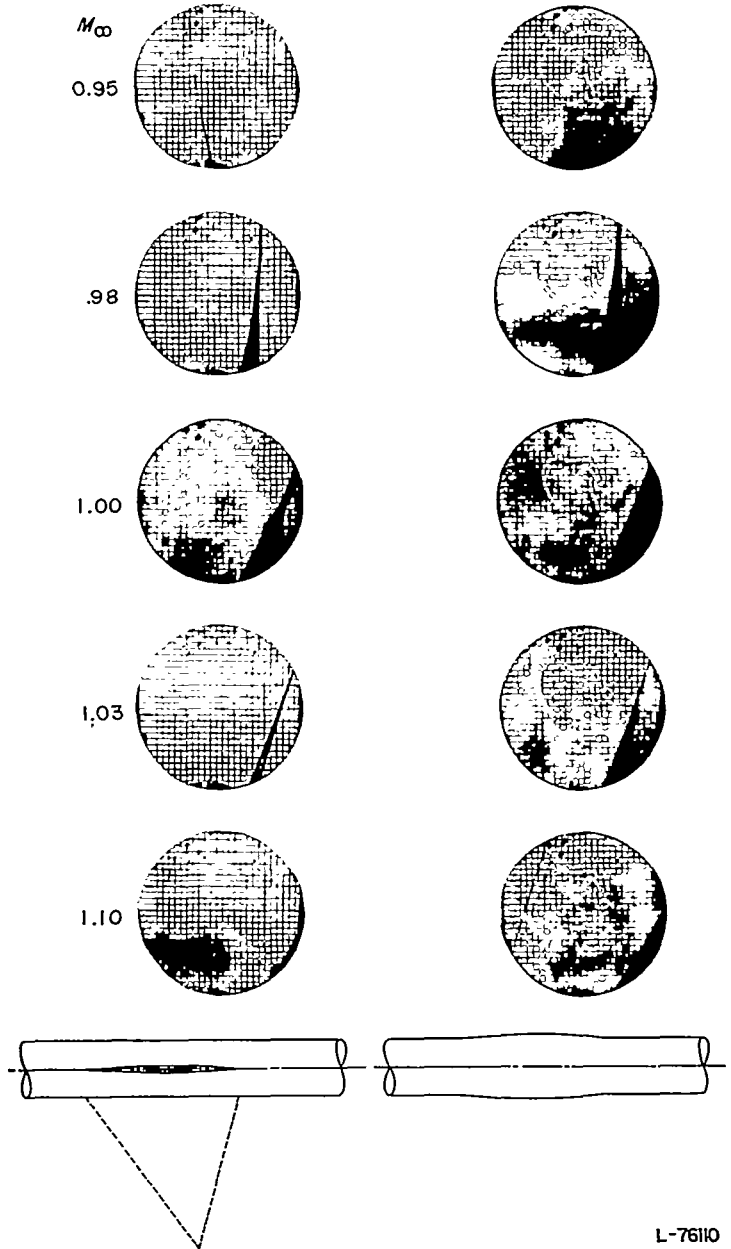


FIGURE 4.—Comparisons of the shock phenomena for the delta-wing and cylindrical-body combination with those for the comparable body of revolution. Side views.

circumferential direction which markedly reduce the variations of the radial deviations. Such effects lead to an essential elimination of the circumferential variations of radial deviations at a relatively short distance from the configuration. Also, any initial circumferential deviations associated with the asymmetry of the wing-body combination are rapidly dissipated with increase in radial distance. As a consequence of the rapid dissipation of both the circumferential deviations and the variations of radial deviations with radial distance, the deviations in a given plane at a short distance from the wing-body configuration are nearly the same as the axially symmetric effects produced by the comparable body of revolution. Such likenesses for the various normal planes are substantiated by the observed similarities of the strong shock formations for the wing-body combination and the comparable body of revolution at a distance from the configurations.

The strong reactions of the flow in the outer regions of the field of the wing-fuselage combination to deviations from axial symmetry, as previously described, converge toward the axis of symmetry and reduce the asymmetrical deviations, even in the immediate region of the wing. These reactions force the inner field into at least an approximate similarity to the axially symmetric field of the body of revolution with the same axial distribution of disturbances, as shown in figure 2.

As the Mach number is increased to supersonic values, the fields of the various disturbances become conical. Also, at these speeds, changes in velocities result in variations of the stream-tube areas. Consequently, the similarities of the shock formations for the wing-body combination and the comparable body of revolution should be progressively lessened as the Mach number is increased beyond the speed of sound.

Drag characteristics.—The close similarity of the shock formations in most regions of the fields for the wing-body combination and the body of revolution with the same axial development of cross-sectional areas suggests that in these regions the energy losses associated with the shocks for the two configurations should be nearly the same. In the locality directly downstream of the wing, the shock losses for the two configurations may differ somewhat; however, the relative effect of such differences should be unimportant. Because of the invariance of the stream-tube areas near a Mach number of 1.0, the fields of flow for these, or any, configurations are relatively extensive. As a result, the greater part of the shock losses for the configurations is due to the large areas of significantly strong shock outside the local region downstream of the wing. Thus, in the local region near the wing, the differences between the shock losses for the wing-body combination and the comparable body should result in relatively small differences of the total losses for the two configurations. Also, because of the low thickness ratio and aspect ratio of the wing and the gradual curvature for the comparable body, the shock-induced separation losses for these configurations should be relatively small, although probably not negligible, and any differences of these losses should be small. Therefore, the drag rise for the combination should be approximately the same as that for the comparable body of revolution.

The measured increments of drag coefficient for the unswept-wing—body combination are the same as those for the comparable body of revolution within the probable accuracy of the data (fig. 3). (The absolute drag coefficients for the comparable configurations differ somewhat, primarily because of differences in skin friction.)

The exact agreement of the drag-rise increments for the unswept-wing—body combination with those for the comparable body of revolution suggests that the secondary separation losses, as well as the primary shock losses, are essentially the same for the two configurations. This apparent agreement can logically be attributed to the fact that the relationships between the shocks and boundary layers for the wing-body combination and the comparable bodies are approximately the same.

The similarity of the drag-rise values for the unswept-wing—body combination and the comparable body of revolution at a Mach number of 1.10 indicates that the perceptible deviations of the shock formations for the two configurations noted at this Mach number (fig. 2 (e)) result in insignificant differences of the shock losses.

DELTA WING AND CYLINDRICAL BODY

Shock phenomena.—Wall Mach number distributions indicate that, as for the unswept-wing—body combination, the flow fields for the delta-wing—body combination at a distance from the configuration are generally almost exactly the same as those for the body of revolution with the same axial distribution of cross-sectional area for all test Mach numbers. The schlieren photographs presented in figure 4 indicate that, in the field above the aft part of the wing, the shocks for the wing-body combination are approximately the same as those for the comparable body. As is the case for the unswept-wing—body combination, the most pronounced deviations of the shock patterns for the comparable configurations probably occur behind the wing.

Drag Characteristics.—The measured variation of the drag coefficient with Mach number for the delta-wing—body combination is the same as that for the comparable body of revolution within the probable accuracy of the measurements (fig. 5). This result was also found for the unswept-wing—body combination.

SWEPT WING AND CYLINDRICAL BODY

Shock phenomena.—Wall Mach number distributions indicate that, as was true for the unswept-wing—body combination, the flow fields for the swept-wing—body combination at a distance from the configuration are almost exactly the same as those for the comparable body of revolution.

The schlieren photographs of figure 6 and reference 1 indicate that near the speed of sound the swept wing produces a weak shock at the trailing edge of the wing-body juncture and a strong shock behind the trailing edge of the juncture. At a Mach number of 1.03, an additional weak shock is also present between these two shocks. The losses in the two weak shocks are insignificant and may be neglected in a comparison of the total shock losses. The side-view schlieren photographs presented in figure 6 indicate that the main shock produced by the wing appears to be approximately the same as the shock caused by the comparable body in the region above the combination. However, the shock produced by the wing is generally somewhat rearward of that produced by the body. At a Mach number of 1.00, this shock for the wing is just visible in the schlieren photograph. Plan-view schlieren surveys not presented herein indicate that near the wing tip the main shock produced by the wing is somewhat different from that caused by the comparable body, particularly at a Mach number of 1.10. (The shock in this region is similar to that for the same wing on the curved body (ref. 1).)

Drag characteristics.—The drag-coefficient increments for the swept-wing—cylindrical-body combination are approximately 0.001 greater than those for the comparable body of

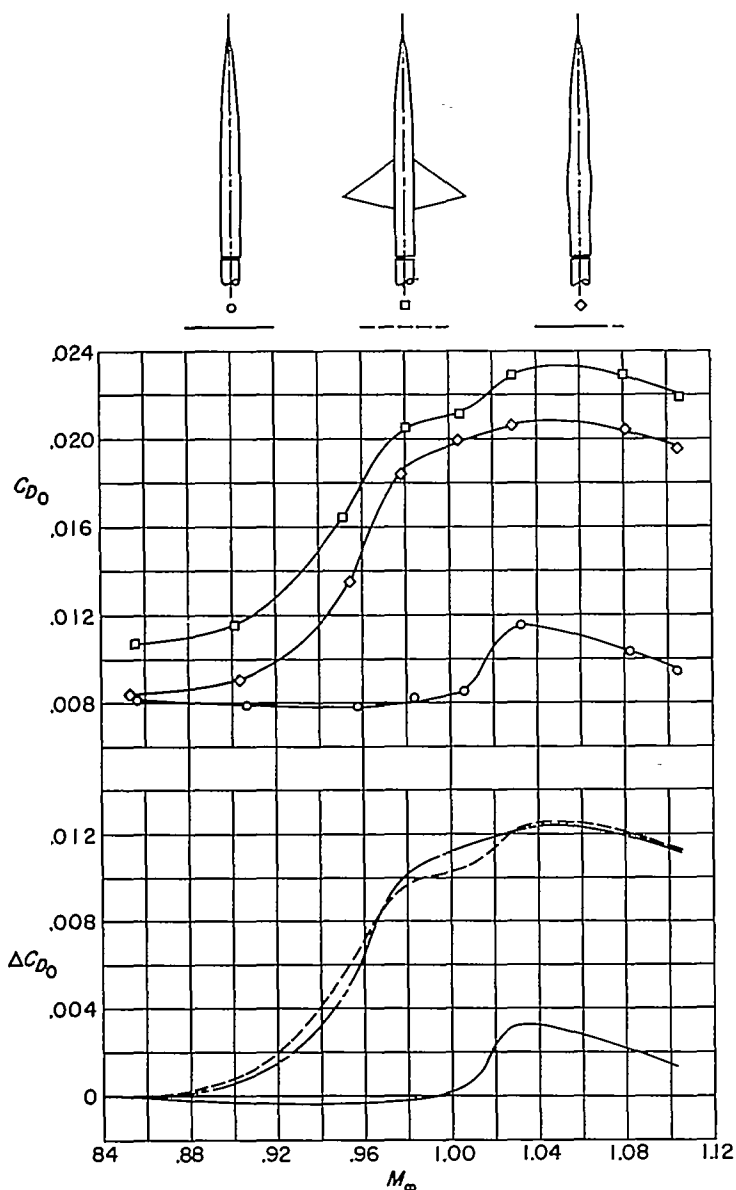


FIGURE 5.—Comparisons of the drag rise for the delta-wing and cylindrical-body combination with that for the comparable body of revolution and the cylindrical body alone.

revolution at Mach numbers up to approximately 1.02 (fig. 7). This difference is approximately the same as the total of the possible maximum errors of the drag measurements. However, if this discrepancy shown is assumed to be real, it can logically be attributed to differences in the shock formations and associated boundary-layer separation. At higher Mach numbers, the differences between the drag increments for the comparable configurations increase primarily because of the more pronounced deviations of the shock formations. The greater differences between the drag-rise increments for this swept-wing—body combination and the comparable body of revolution in comparison with those for the unswept wing may be attributed primarily to the greater thickness ratio and smaller taper of the swept wing.

SWEPT WING AND CURVED BODY

Shock phenomena.—The shock formations as indicated in the side-view schlieren photograph for the swept-wing—

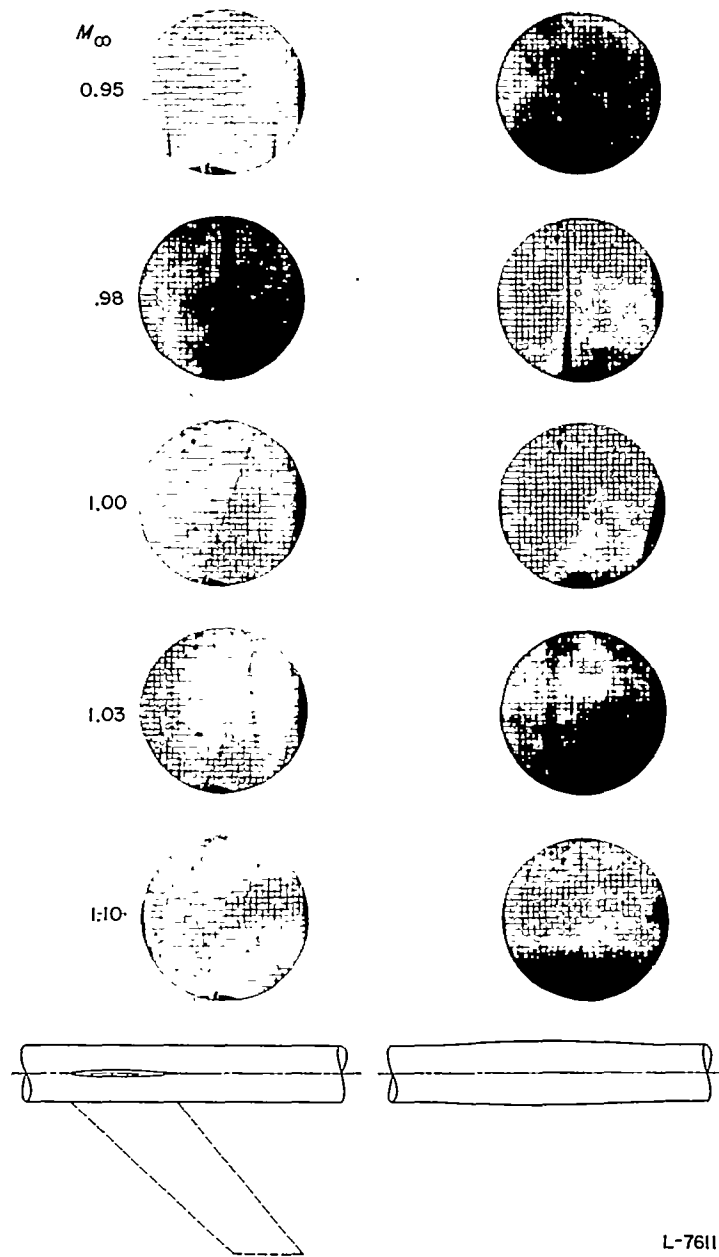


FIGURE 6.—Comparisons of the shock phenomena for the swept-wing and cylindrical-body combination with those for the comparable body of revolution. Side views.

curved-body combination (fig. 8) are similar to, but apparently stronger than, those for the swept-wing—cylindrical-body configuration (fig. 6). The differences between the shock formations produced by the swept-wing—curved-body configuration (fig. 8 and ref. 1) and those for the comparable body of revolution are also similar to the differences for the swept-wing—cylindrical-body combination.

Drag characteristics.—Combination of the swept wing and curved body results in a severe adverse drag interference between the wing and body near the speed of sound (fig. 9). The drag-coefficient rise for the swept wing in combination with this body near the speed of sound is approximately 0.012 as compared with a value of 0.004 for the wing in conjunction with the essentially interference-free cylindrical body. (See figs. 7 and 9.) (These differences in the drag-rise values may be due in part to the difference in the

L-76111

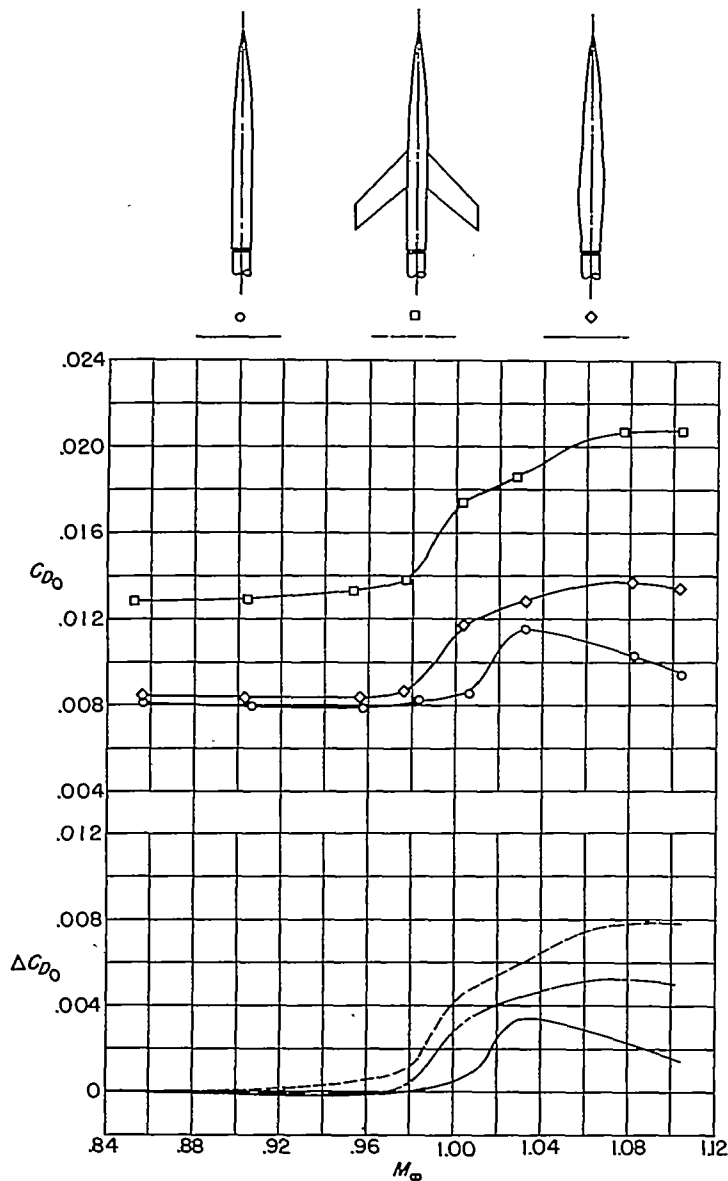


FIGURE 7.—Comparisons of the drag rise for the swept-wing and cylindrical-body combination with that for the comparable body of revolution and the cylindrical body alone.

maximum body diameter as well as the large variation of the curvature of the afterbody.)

The pronounced drag-rise increments for the swept-wing and curved-body configuration are approximately 0.003 greater than those for the comparable body near the speed of sound (fig. 9). The maximum drag rise for the combination, as measured at a Mach number of 1.03, is approximately 15 percent greater than that for the comparable body of revolution. These differences can be attributed to the same factors which caused the similar but smaller differences for the swept-wing—cylindrical-body combination.

Of particular importance is the fact that the relative increase in the drag rise for the swept-wing—curved-body combination as compared with that for the swept-wing—cylindrical-body configuration is approximately the same as the relative increase for the comparable bodies of revolution.

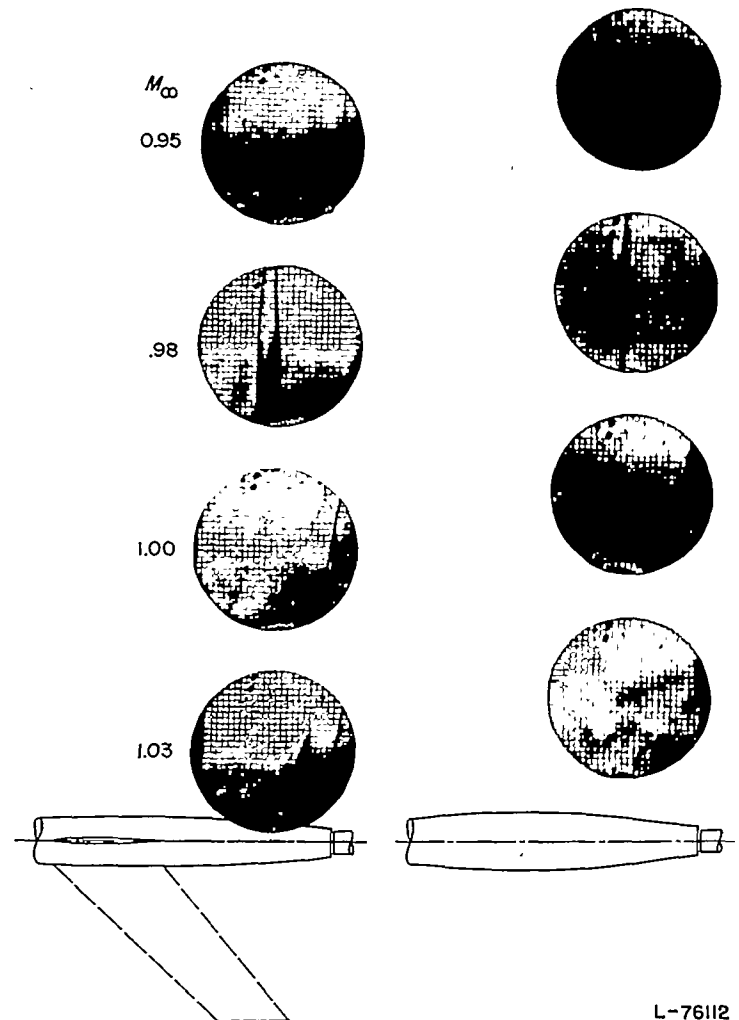


FIGURE 8.—Comparisons of the shock phenomena for the swept-wing and curved-body combination with those for the comparable body of revolution. Side views.

GENERALIZATION

The results presented indicate that, near the speed of sound, the shock formations and the associated drag-rise characteristics for the various wing and central-body combinations investigated are, to the first order, the same as those for the bodies of revolution with the same axial developments of cross-sectional areas normal to the airstream. These bodies of revolution are simple axial developments of cross-sectional areas. Therefore, on the basis of the results presented, it may logically be concluded that, near the speed of sound, the zero-lift drag rise of a low-aspect-ratio thin-wing—body combination is primarily dependent on the axial development of cross-sectional areas normal to the airstream. It follows that the drag rise for any such configuration is approximately the same as that for any other with the same development of cross-sectional areas.

It may be assumed that this concept is also valid for wings alone, wings or wing-body combinations with moderate twist or camber, or yawed configurations; however, no directly

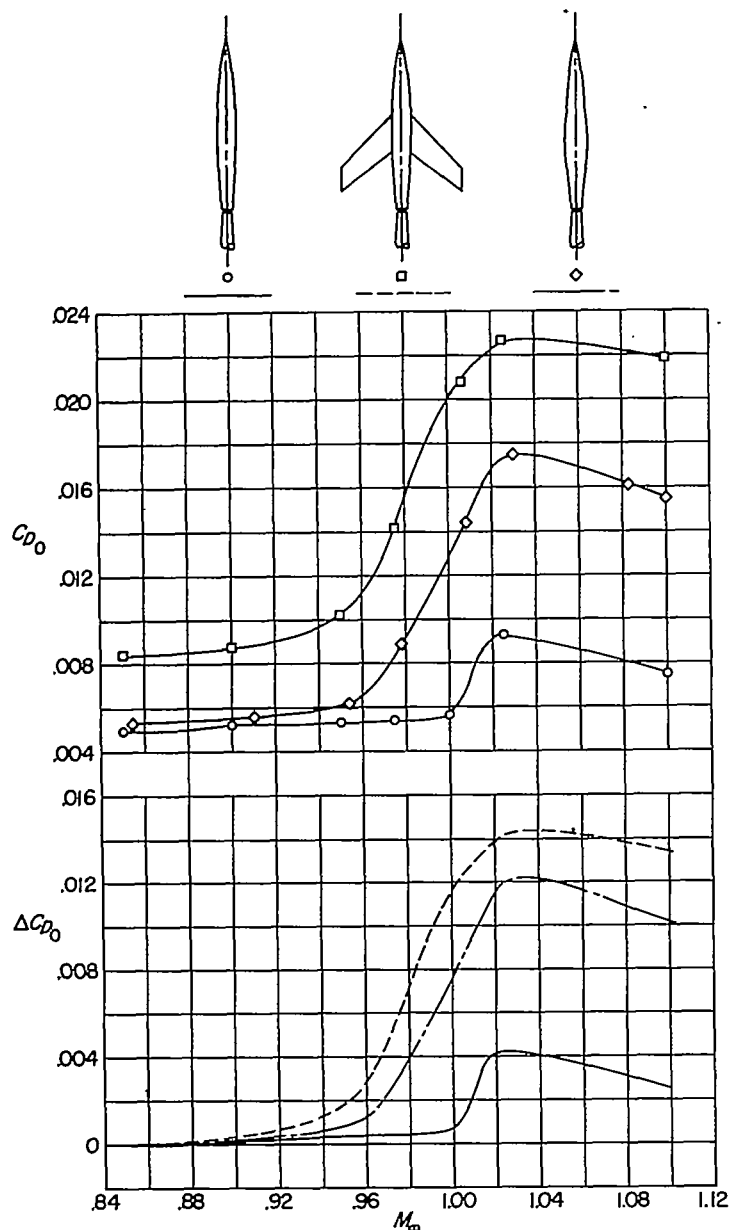


FIGURE 9.—Comparisons of the drag rise for the swept-wing and curved-body combination with that for the comparable body of revolution and the curved body alone.

comparable experimental results are available to substantiate these conjectures. Linear theory (ref. 4) and experiments (ref. 5) have indicated that a similar relation is valid for slender noncircular bodies at supersonic as well as at transonic speeds. A similar relationship for the wave drag of wing-body combinations is implicit in the linear supersonic theory of reference 6.

APPLICATIONS OF TRANSONIC DRAG-RISE CONCEPT

Correlation of drag-rise characteristics.—The accuracy of a quantitative correlation of the drag rise of a conventional wing-body combination by using the proposed concept should be lessened by increasing the thickness ratio, aspect ratio, or taper ratio of the wing. The effects of enlarging these variables should become greater as the Mach number is increased beyond the speed of sound. The results presented

herein indicate that usual variations of the shape of the body should have little effect on the accuracy of a quantitative correlation. The magnitudes of the section thickness ratios, aspect ratios, and taper ratios for the wings of contemporary transonic and supersonic aircraft generally lie between the values for the unswept and swept wings used in the present investigation. It may be assumed, therefore, that the accuracies of quantitative correlations of the drag-rise increments for these real configurations would be between those for the models investigated.

Because of the lack of knowledge as to the effects of detailed changes in the axial developments of cross-sectional areas on the drag-rise characteristics, quantitative correlations as presented herein are not generally feasible. However, it has been possible to correlate qualitatively all the available reliable drag-rise results for wings and wing-body combinations (refs. 7 and 8, for example) by use of the available information for the effects of general changes in body shape on the transonic drag rise (refs. 2 and 9, for example). It appears that the concept should be generally useful in comparing the approximate relative effects of various design alterations.

A preliminary analysis of the available information defining the effects of nacelle position on the interference between the nacelle and the wing at transonic speeds (ref. 10) indicated that this interference can be correlated qualitatively, at least, on the basis of the concept proposed. However, further specific experimental comparisons are required to define the exact applicability of this concept to the correlation of such interference.

An idea, similar to that proposed herein, was presented in reference 11 for predicting the critical speeds of wing-body combinations.

Interpretation of variations of drag-rise characteristics.—Analyses of the available drag-rise characteristics indicate that variations in wing configurations which result in less rapid rates of development of cross-sectional areas, as well as reductions of the relative magnitude of the maximum areas, decrease the drag-rise increments near the speed of sound. For example, the rates of development and maximum value of the cross-sectional areas for the swept wing of the present investigation are less than those for the unswept wing (table II). As a result, the drag rise for the swept wing is less pronounced (figs. 3 and 7).

Reversing the unswept wing to form the delta wing (fig. 1) reduced the rate of expansion of cross-sectional areas for the forward part of the wing but increased the rate of contraction of areas for the rearward part (table II). These variations resulted in increases of the drag-rise increments for the delta wing (figs. 3 and 5). On the basis of this comparison, as well as the results presented in reference 2, it may be assumed that, near the speed of sound, a given rate of decrease in cross-sectional area generally results in a greater drag rise than does a similar increase.

On the basis of the proposed concept, adverse zero-lift drag interference between wings and bodies, as for the swept-wing—body combination investigated (fig. 9), can generally

be attributed basically to greater rates of development of the cross-sectional areas for the combinations compared with those for the components (table II). These more rapid variations of area generally result in higher induced velocities and considerably stronger shocks in the fields of the combinations. (For example, compare figs. 6 and 8.) Obviously the interference drags, associated with the increased shock losses, are directly produced by changes in the pressures on the body and wing. (For example, see ref. 1.) The favorable effects of various changes in body shape on the interference between the wing and body, as shown in reference 8, can be attributed to reductions in the rates of development of the cross-sectional areas.

Reductions of the drag-rise increments of wing-body combinations.—On the basis of the concept proposed, it would be expected that indenting the body of a wing-body combination, so that the combination has the same axial distribution of cross-sectional area as the original body alone, would result in a large reduction or elimination of the drag rise associated with the wing. This type of indentation was used on the cylindrical body investigated in combination with the unswept, delta, and swept wings. (See fig. 1.)

As shown in figure 10, indenting the body reduced the drag-rise increments associated with the unswept and delta wings by approximately 60 percent near the speed of sound. This alteration eliminated the drag rise associated with the swept wing at Mach numbers up to 1.04. At higher Mach numbers, the effects of the indentations gradually decreased. Even for these relatively unconventional configurations, the proposed concept predicts correctly the qualitative effects of design modifications on the drag-rise characteristics near the speed of sound.

The incomplete effects of indenting the bodies with the unswept and delta wings may be attributed in part to local induced flows and to the displacement of the stream tubes by the boundary layer, which were neglected in the design of the indentations. For the swept wing, these effects are less important because of the more gradual axial development of the indentation. Minor modifications of the indentations of the body to account for these factors should further reduce the drag-rise increments associated with the unswept and delta wings. The reductions of the effects of these indentations at supersonic Mach numbers are associated with the change in the nature of the flow field at the higher speeds, as described in the discussion of the shock phenomena for the unswept wing.

At lift coefficients up to approximately 0.3, the indentations of the bodies result in drag reductions similar to those shown. Although these indentations have not completely eliminated the near-sonic drag-rise increments associated with all the wings investigated, they have at least greatly reduced the increments in every case.

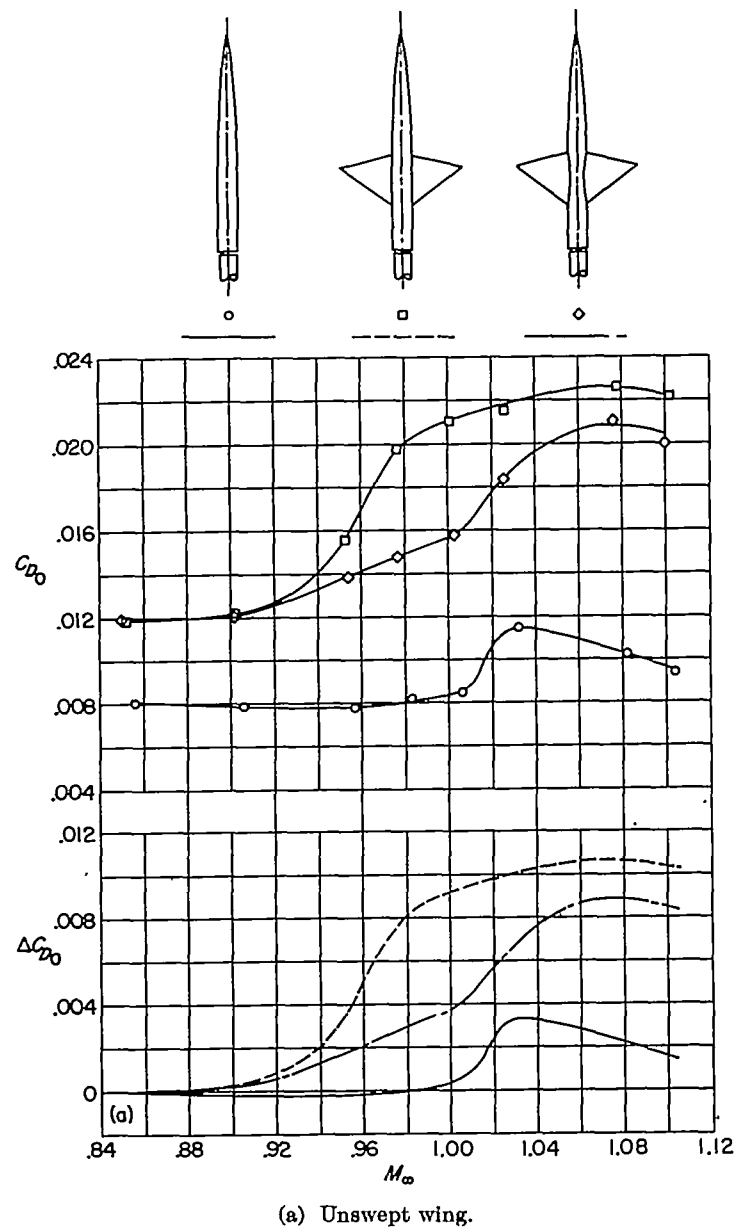
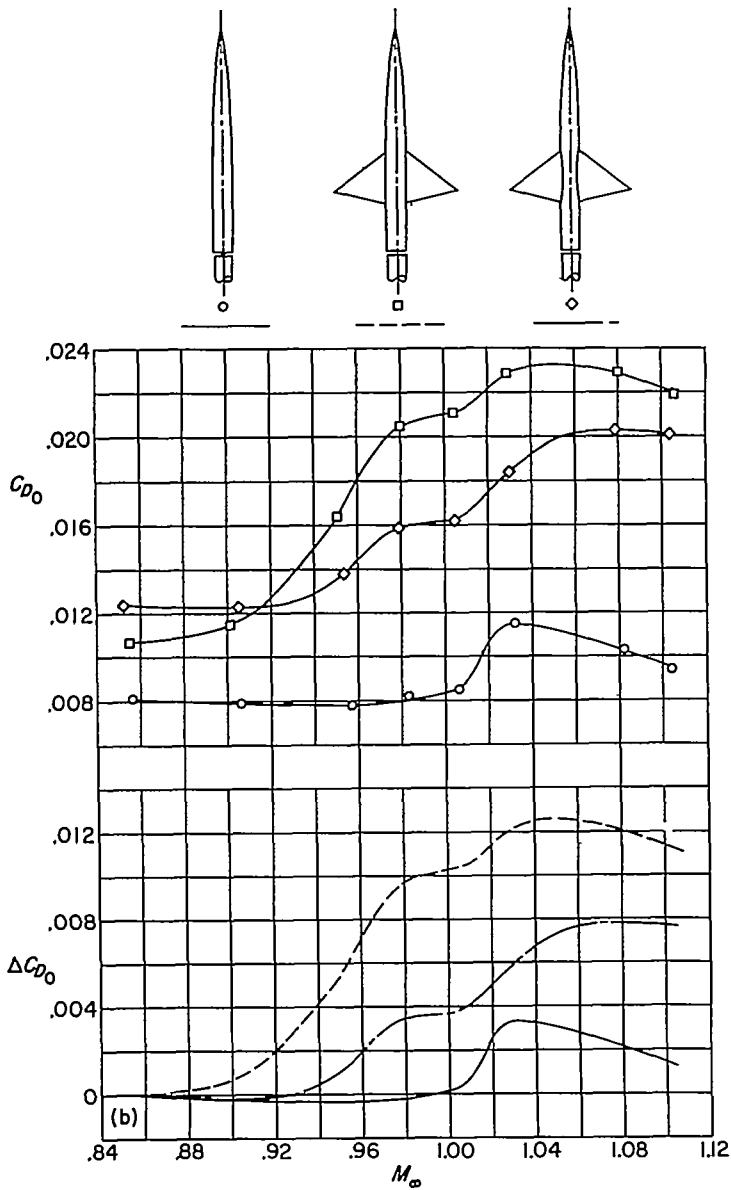


FIGURE 10.—The effects on transonic drag obtained by indenting the bodies of three wing-body combinations.

On the basis of this concept it would be expected that the minimum transonic drag rise for an airplane could be obtained by shaping the fuselage so that the development of cross-sectional area for the airplane approaches that for a low-drag body of revolution with the highest feasible fineness ratio.

CONCLUSIONS

Comparisons of the shock phenomena and drag-rise increments for representative wing and central-body combinations with those for bodies of revolution having the same



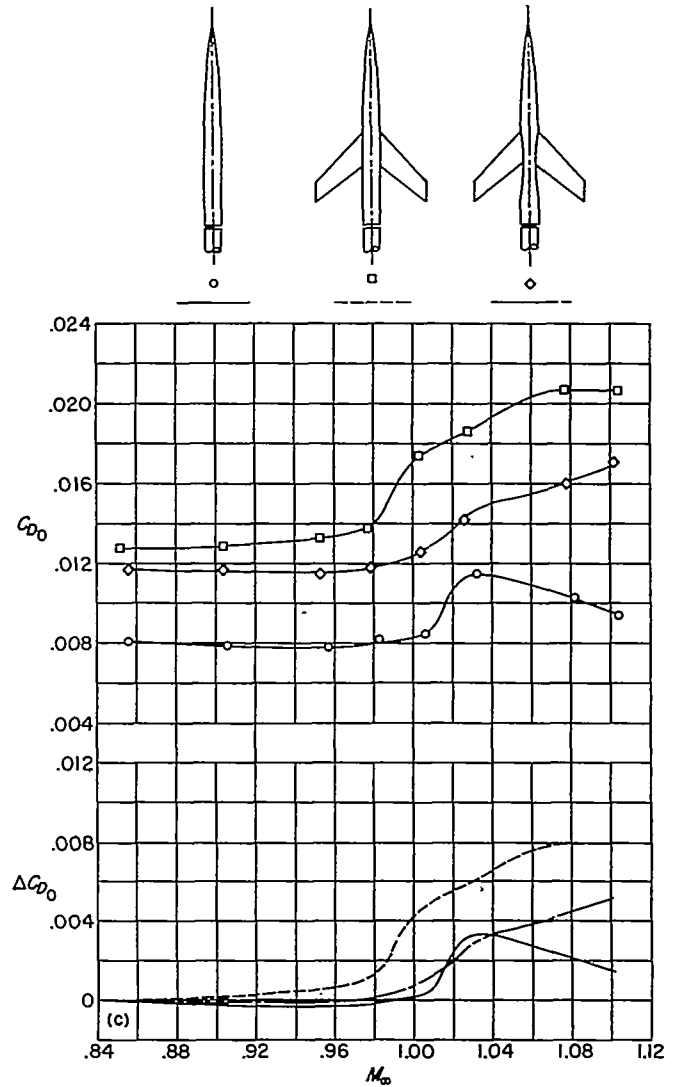
(b) Delta wing.

FIGURE 10.—Continued.

axial developments of cross-sectional areas normal to the airstream have indicated the following conclusions:

1. The shock phenomena and drag-rise increments measured for these representative wing and central-body combinations at zero lift near the speed of sound are essentially the same as those for the comparable bodies of revolution.

2. Near the speed of sound, the zero-lift drag rise of a low-aspect-ratio thin-wing—body combination is primarily dependent on the axial development of the cross-sectional areas normal to the airstream. Therefore, it follows that



(c) Swept wing.

FIGURE 10.—Concluded.

the drag rise for any such configuration is approximately the same as that for any other with the same development of cross-sectional areas.

Further results have indicated that indenting the bodies of three representative wing-body combinations, so that the axial developments of cross-sectional areas for the combinations were the same as for the original body alone, greatly reduced or eliminated the zero-lift drag-rise increments associated with wings near the speed of sound.

LANGLEY AERONAUTICAL LABORATORY,
 NATIONAL ADVISORY COMMITTEE FOR AERONAUTICS,
 LANGLEY FIELD, VA., August 1, 1952.

REFERENCES

1. Whitcomb, Richard T., and Kelly, Thomas C.: A Study of the Flow Over a 45° Sweptback Wing-Fuselage Combination at Transonic Mach Numbers. NACA RM L52D01, 1952.
2. Thompson, Jim Rogers, and Kurbjun, Max C.: Drag Measurements at Transonic Speeds of Two Bodies of Fineness Ratio 9 With Different Locations of Maximum Body Diameter. NACA RM L8A28b, 1948.
3. Busemann, Adolf: Application of Transonic Similarity. NACA TN 2687, 1952.
4. Graham, Ernest W.: The Pressure on a Slender Body of Non-Uniform Cross-Sectional Shape in Axial Supersonic Flow. Rep. No. SM-13346-A, Douglas Aircraft Co., Inc., July 20, 1949.
5. Stoney, William E., Jr., and Putland, Leonard W.: Some Effects of Body Cross-Sectional Shape, Including a Sunken-Canopy Design, on Drag As Shown by Rocket-Powered-Model Tests at Mach Numbers From 0.8 to 1.5. NACA RM L52D07, 1952.
6. Hayes, Wallace D.: Linearized Supersonic Flow. Rep. No. AL-222, North American Aviation, Inc., June 18, 1947.
7. Nelson, Warren H., and McDevitt, John B.: The Transonic Characteristics of 22 Rectangular, Symmetrical Wing Models of Varying Aspect Ratio and Thickness. NACA TN 3501, 1955. (Supersedes NACA RM A51A12.)
8. Pepper, William B.: The Effect on Zero-Lift Drag of an Indented Fuselage or a Thickened Wing-Root Modification to a 45° Sweptback Wing-Body Configuration As Determined by Flight Tests at Transonic Speeds. NACA RM L51F15, 1951.
9. Thompson, Jim Rogers: Measurements of the Drag and Pressure Distribution on a Body of Revolution Throughout Transition From Subsonic to Supersonic Speeds. NACA RM L9J27, 1950.
10. Pepper, William B., Jr., and Hoffman, Sherwood: Comparison of Zero-Lift Drags Determined by Flight Tests at Transonic Speeds of Symmetrically Mounted Nacelles in Various Spanwise Positions on a 45° Sweptback Wing and Body Combination. NACA RM L51D06, 1951.
11. Robinson, Russell G., and Wright, Ray H.: Estimation of Critical Speeds of Airfoils and Streamline Bodies. NACA ACR, Mar. 1940.